JOINT SPARSITY BASED SPARSE SUBSPACE CLUSTERING FOR HYPERSPECTRAL IMAGES

Shaoguang Huang[1]*, Hongyan Zhang*[2] *and Aleksandra Pižurica*[1]

[1]Department of Telecommunications and Information Processing, TELIN-IPI-imec, Ghent University, Belgium
[2]The State Key Lab. of Inform. Engineering in Surveying, Mapping, and Remote Sensing, Wuhan University, China

ABSTRACT

Sparse subspace clustering (SSC) has been widely applied in remote sensing demonstrating excellent performance. Recent extensions incorporate spatial information, typically via smoothness-enforcing regularization. We propose an alternative approach: a joint sparsity SSC model, where pixels within a local region are enforced to select a common set of samples in the subspace-sparse representation. The corresponding optimization problem is solved by the alternating direction method of multipliers (ADMM). Experimental results on real data show a significant improvement over SSC and related state-of-the-art methods.

Index Terms— Hyperspectral images, joint sparsity, sparse subspace clustering, super-pixels segmentation.

1. INTRODUCTION

Hyperspectral images (HSIs), captured with hundreds of spectral bands offer richer information about the imaged objects than the multispectral images. Therefore, HSIs have become a powerful and valuable tool for various applications including defense and security [1], agriculture [2] and environmental monitoring [3]. When training samples are unavailable, clustering of a HSI, known as the problem of separating the pixels into different groups where the pixels in the same group are more similar to each other than to those in other groups, is usually regarded as a fundamental step in all these applications. However, due to the large spectral variability and complex structure, clustering of HSIs is being a very challenging task [4].

Traditional clustering methods such as k-means [5], fuzzy c-means (FCM) [6] and generalized principal component analysis (GPCA) [7] have been widely used in remote sensing. However, directly applying such methods on HSIs often produces the clustering maps with a large amount of impulse noise, due to the limited discriminative information in spectral domain, complexity of ground objects and large diversity of spectral signatures in the same class [8].

In recent years, sparse subspace clustering (SSC) [9] has emerged as an effective method for HSI clustering, providing the current state-of-the-art performance [4, 10–12]. SSC relies on a self-representation model where the input matrix is employed as a dictionary and states that for a given sample in a union of subspaces, there exist a sparse representation vector whose non-zero entries correspond to the samples in the same subspace [9], named as subspace-sparse representation. As the subspace-sparse representation of the input matrix reflects the memberships of each sample, it is employed to build a similarity matrix which is further applied within the spectral clustering framework [13].

The performance of SSC is limited by the fact that it treats each pixel independently without considering the spatial distribution of data points. A number of approaches have been proposed to exploit spatial information in HSIs and achieved a significant improvement over SSC [4, 11, 12, 14]. The approach of [4] imposes a smoothness constraint on the neighbouring sparse coefficients within square patches. Another ℓ_2-norm based spatial regularizer acting on the coefficients of horizontally and vrtically adjacent pixels was proposed in [11] to promote piecewise smoothness of sparse coefficients. An object-oriented SSC method was proposed in [14], which extracts spectral-spatial features in each segmented object by a reweighted mass center learning method. A kernel version of SSC incorporating with a max pooling of coefficient matrix was presented in [12].

From another perspective, we propose a joint sparsity based SSC (JSSC) model with the purpose of building a more accurate similarity matrix with the inherent spatial information of HSI. Specifically, we enforce the pixels in each homogeneous region to share a common set of samples in the subspace-sparse representation by a joint sparsity constraint. The homogeneous regions are obtained by a super-pixel segmentation technique, which is able to segment HSIs into a number of non-overlapping super-pixels with an adaptive

This work was supported by the FWO project: G.OA26.17N Dictionary Learning and Distributed Inference for the Processing of Large-scale Heterogeneous Image Data (DOLPHIN).

shape and size. Each super-pixel is typically comprised of the same material which means the spectral signatures in one super-pixel are similar to each other. We assume that those spectral signatures lie in the same subspace. In order to build such a relationship, we integrate a joint sparsity constraint for each super-pixel with the SSC model, which greatly promotes the graph connectivity. In order to solve the resulting optimization problem, we derive an iterative solver based on the alternating direction method of multipliers (ADMM). The proposed method was validated on real data. Experimental results demonstrate the effectiveness of JSSC with a significant performance improvement over the existing methods in terms of overall accuracy.

The rest of this paper is organized as follows. Section 2 briefly introduces the SSC model. Section 3 describes the proposed JSSC model and the optimization algorithm. Section 4 presents the experimental results on real data and Section 5 concludes the paper.

2. SSC MODEL

We assume the size of a 3-D HSI is $M \times N \times B$, where M, N represents the height and width of the data respectively and B denotes the number of bands. The data is first flattened to a 2-D matrix $\mathbf{Y} \in \mathbb{R}^{B \times MN}$ where each column is a spectral signature. With the assumption that each pixel in a union of subspaces can be sparsely represented as a linear or affine combination of the others from the same subspace [9, 15], the sparse matrix $\mathbf{C} \in \mathbb{R}^{MN \times MN}$ of $\mathbf{Y}$ can be derived by:

$$\begin{aligned} &\arg\min_{\mathbf{C}} \|\mathbf{C}\|_1 + \frac{\lambda}{2}\|\mathbf{Y} - \mathbf{Y}\mathbf{C}\|_F^2 \\ &s.t.\ \ diag(\mathbf{C}) = \mathbf{0},\ \ \mathbf{1}^T\mathbf{C} = \mathbf{1}^T, \end{aligned} \tag{1}$$

where $\|\mathbf{C}\|_1 = \sum_i \sum_j |C_{ij}|$ and λ is a parameter which controls the balance between the data representation error and the matrix sparsity. The first constraint is used to avoid the trivial solution of representing a sample by itself and the second constraint indicates the case of affine subspace.

The model in (1) can be solved by ADMM [16]. The nonzero entries of $\mathbf{C}$ specify which data points will be selected in the subspace-sparse representation. Therefore, matrix $\mathbf{C}$ reflects the relationships between each pixel in $\mathbf{Y}$. Then we can obtain a similarity matrix $\mathbf{W} \in \mathbb{R}^{MN \times MN}$ by

$$\mathbf{W} = |\mathbf{C}| + |\mathbf{C}|^T. \tag{2}$$

With spectral graph theory, the clustering results can be achieved by applying k-means to a subset of eigenvectors of the Laplacian matrix $\mathbf{L} = \mathbf{D} - \mathbf{W}$ where $\mathbf{D} \in \mathbb{R}^{MN \times MN}$ is a diagonal matrix with $D_{ii} = \sum_j W_{ij}$ [13].

3. PROPOSED METHOD

SSC treats each pixel of $\mathbf{Y}$ independently in the subspace-sparse representation. Various factors such as limited discriminative information in spectral domain, noise and large diversity of spectral signatures belonging to the same class in HSIs [4], affect the construction of the similarity matrix, deteriorating thereby spectral clustering performance. In practice, pixel values are spatially correlated, which means that the pixels within a local region typically belong to the same class [17–20]. Here, we exploit the spatial information with a joint sparsity constraint to preserve the dependencies between HSI pixels in a local region.

3.1. JSSC model

Suppose that we segment a HSI into p non-overlapping super-pixels [21]. Each super-pixel is regarded as a homogeneous region belonging to a particular class. We assume that each pixel within the same super-pixel selects the same set of pixels in the data representation but with different coefficients. The proposed JSSC model can be described as follows:

$$\begin{aligned} &\arg\min_{\mathbf{C}} \sum_{i=1}^{p} w_i \|\mathbf{C_i}\|_{1,2} + \frac{\lambda}{2}\|\mathbf{Y} - \mathbf{Y}\mathbf{C}\|_F^2 \\ &s.t.\ \ diag(\mathbf{C}) = \mathbf{0},\ \ \mathbf{1}^T\mathbf{C} = \mathbf{1}^T, \end{aligned} \tag{3}$$

where $\mathbf{C_i} \in \mathbb{R}^{MN \times n_i}$ is a sparse matrix that corresponds to the n_i pixels in i-th super-pixel; $\|\mathbf{C_i}\|_{1,2}$ is the $\ell_{1,2}$ norm defined as $\sum_{j=1}^{MN} \|\mathbf{c_i^j}\|_2$. Here $\mathbf{c_i^j}$ is the j-th row of $\mathbf{C_i}$ and w_i is a normalized weight defined as:

$$w_i = \frac{\sqrt{n_i/p}}{\sum_{i=1}^{p} \sqrt{n_i/p}}. \tag{4}$$

to make the joint sparsity constraint in each super-pixel balanced. The first term with $\ell_{1,2}$ norm enforces the pixels in one super-pixel to select a common set of samples in the data representation, which promotes the connectivity of the graph within the local region. This model can be efficiently solved by ADMM which will be described in detail next.

Once we obtain the sparse matrix $\mathbf{C}$, the similarity matrix can be calculated by (2) and further applied in the spectral clustering method to yield the clustering results in the same way as SSC.

3.2. Optimization method

In this section we give the optimization method in detail based on the ADMM. We first introduce an auxiliary variable $\mathbf{A}$ and reformulate the problem (3) equivalently as:

$$\begin{aligned} &\arg\min_{\mathbf{C},\mathbf{A}} \sum_{i=1}^{p} w_i \|\mathbf{A_i}\|_{1,2} + \frac{\lambda}{2}\|\mathbf{Y} - \mathbf{Y}\mathbf{C}\|_F^2 \\ &s.t.\ \ diag(\mathbf{C}) = \mathbf{0},\ \ \mathbf{1}^T\mathbf{C} = \mathbf{1}^T,\ \ \mathbf{C} = \mathbf{A} \end{aligned} \tag{5}$$

The augmented Lagrangian function $f_\mu(\mathbf{C}, \mathbf{A}; \mathbf{Y_1}, \mathbf{Y_2}, \mathbf{Y_3})$ can be derived as follows:

$$\sum_{i=1}^{p} w_i \|\mathbf{A_i}\|_{1,2} + \frac{\lambda}{2}\|\mathbf{Y} - \mathbf{YC}\|_F^2 + \langle \mathbf{Y_1}, \mathbf{1}^T\mathbf{C} - \mathbf{1}^T\rangle + \langle \mathbf{Y_2}, \mathbf{C} - \mathbf{A}\rangle + \langle \mathbf{Y}_3, diag(\mathbf{C})\rangle + \frac{\mu}{2}(\|\mathbf{1}^T\mathbf{C} - \mathbf{1}^T\|_F^2 + \|\mathbf{C} - \mathbf{A}\|_F^2 + \|diag(\mathbf{C})\|_2^2), \quad (6)$$

where $\mathbf{Y}_1, \mathbf{Y}_2$ and $\mathbf{Y}_3$ are the Lagrange multipliers, and μ is a weighting parameter. Due to the separable structure of f_μ, we can solve each of $\mathbf{C}$ and $\mathbf{A}$ separately by fixing one when solving another. Different steps are described as following.

3.2.1. *Update C*

The objective function with respect to $\mathbf{C}$ is given by:

$$\mathbf{C}^{k+1} = \arg\min_{\mathbf{C}} \frac{\lambda}{2}\|\mathbf{Y} - \mathbf{YC}\|_F^2 + \frac{\mu^k}{2}(\|\mathbf{1}^T\mathbf{C} - \mathbf{1}^T + \frac{\mathbf{Y}_1^k}{\mu^k}\|_F^2 + \|\mathbf{C} - \mathbf{A}^k + \frac{\mathbf{Y}_2^k}{\mu^k}\|_F^2 + \|diag(\mathbf{C}) + \frac{\mathbf{Y}_3^k}{\mu^k}\|_2^2) \quad (7)$$

By setting the first-order derivative to zero, a closed form solution in a column-wise manner is obtained as

$$\mathbf{c}_i^{k+1} = (\lambda\mathbf{Y}^T\mathbf{Y} + \mu^k(\mathbf{e}_i\mathbf{e}_i^T + \mathbf{I} + 1))^{-1}(\lambda\mathbf{Y}^T\mathbf{y}_i + \mu^k(\boldsymbol{\alpha}_i^k + 1) - y_{1_i}^k\mathbf{1} - \mathbf{y}_{2_i}^k - y_{3_i}^k\mathbf{e}_i), \quad (8)$$

where $y_{1_i} \in \mathbb{R}, \mathbf{y}_{2_i} \in \mathbb{R}^{MN}$ and $y_{3_i} \in \mathbb{R}$ are the the i-th element or vector of $\mathbf{Y}_1, \mathbf{Y}_2$ and $\mathbf{Y}_3$, respectively.

3.2.2. *Update A*

The objective function with respect to $\mathbf{A}$ is:

$$\mathbf{A}^{k+1} = \arg\min_{\mathbf{A}} \sum_{i=1}^{p} w_i\|\mathbf{A_i}\|_{1,2} + \frac{\mu^k}{2}\|\mathbf{C}^{k+1} - \mathbf{A} + \frac{\mathbf{Y}_2^k}{\mu^k}\|_F^2 \quad (9)$$

which can be separated into p sub-problems of the form

$$\arg\min_{\mathbf{A}_i} \; w_i\|\mathbf{A_i}\|_{1,2} + \frac{\mu^k}{2}\|\mathbf{C}_i^{k+1} - \mathbf{A}_i + \frac{\mathbf{Y}_{2_i}^k}{\mu^k}\|_F^2, \quad (10)$$

where $\mathbf{Y}_{2_i} \in \mathbb{R}^{MN \times n_i}$ is a matrix with each column indexed by the pixels in i-th super-pixel. This problem can be solved by a shrinkage operator [22, 23].

3.2.3. *Update other parameters*

The next step is to update the multipliers $\mathbf{Y}_1, \mathbf{Y}_2$ and μ, which can be achieved by

$$\mathbf{Y}_1^{k+1} = \mathbf{Y}_1^k + \mu^k(\mathbf{1}^T\mathbf{C}^{k+1} - \mathbf{1}^T) \quad (11)$$

$$\mathbf{Y}_2^{k+1} = \mathbf{Y}_2^k + \mu^k(\mathbf{C}^{k+1} - \mathbf{A}^{k+1}) \quad (12)$$

$$\mathbf{Y}_3^{k+1} = \mathbf{Y}_3^k + \mu^k diag(\mathbf{C}) \quad (13)$$

$$\mu^{k+1} = \rho\mu^k, \quad (14)$$

Table 1. Clustering accuracy for *Indian Pines*.

Class name	FCM	k-means	SSC	L2-SSC	JSSC
Corn-notill	62.39	69.85	60.00	61.09	**74.03**
Grass-trees	94.66	53.84	98.36	99.32	**100**
Soybean-notill	44.13	0	76.91	79.37	**86.20**
Soybean-mintill	63.83	57.59	50.68	54.89	**87.79**
OA(%)	65.34	50.17	65.11	67.78	**86.40**
κ	0.5118	0.2833	0.5296	0.5629	**0.8069**

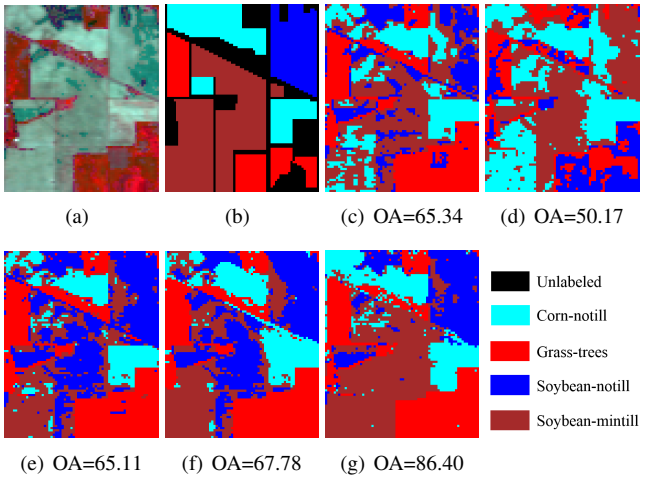

Fig. 1. *Indian Pines* image. (a) False color image, (b) Ground truth, and Clustering maps of (c) FCM (d) k-means. (e) SSC. (f) L2-SSC. (g) JSSC.

where $\rho \geq 1$ is a parameter that controls the convergence speed of the optimization. The three updating steps are executed iteratively until the stop criterion is satisfied.

4. EXPERIMENTAL RESULTS AND ANALYSIS

Experiments are conducted on two real HSIs to validate the performance of the proposed method. The results of two widely used clustering methods FCM [6] and k-means [5], and state-of-the-art methods SSC [9] and L2-SSC [11] are reported for comparison. Two common performance measures: overall accuracy (OA) and Kappa coefficient (κ) are used for quantitative assessment of the clustering performances. The optimal λ of JSSC is set as 10 experimentally.

4.1. Experiments on real data

Experiment 1 was conducted on the *Indian Pines*, which was acquired by the Airborne/Visible Infrared Imaging Spectrometer (AVIRIS) sensors from the North-western Indiana in June 1992. A subimage with the size of 85×70 is cut as the test data as it is done in [4], which has in total 4 classes. The false color image and ground truth are shown in Fig. 1 (a) and (b).

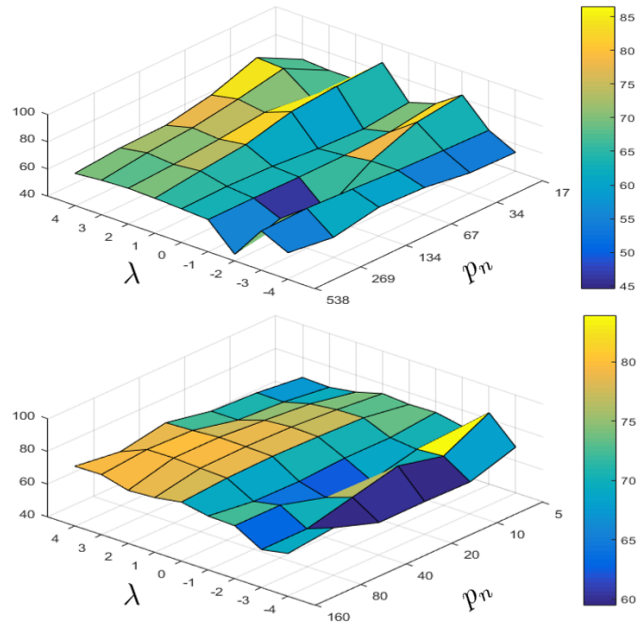

Fig. 2. Grid search of λ and p for JSSC (the λ-axis is in log_{10} and p_n is defined by $p/M/N \times 10^4$). Top: *Indian Pines*; Bottom: *Pavia University*.

Table 2. Clustering accuracy for *Pavia University*.

Class name	FCM	k-means	SSC	L2-SSC	JSSC
Asphalt	0	0	6.12	0	**11.76**
Meadows	86.33	78.91	57.55	94.27	**99.35**
Trees	60.32	66.67	95.24	84.13	**98.41**
Metal	61.37	58.63	98.10	97.34	**99.77**
Bare Soil	40.72	44.43	39.12	51.78	**68.50**
Bitumen	**100**	**100**	98.49	97.21	99.07
Brick	1.06	0	0	**39.36**	0
Shadows	**100**	**100**	82.55	99.72	89.02
OA(%)	58.53	58.60	61.51	71.61	**79.35**
κ	0.5032	0.5	0.5378	0.6554	**0.7404**

The parameters for each reference method were carefully tuned and the best results are reported in Table 1 and Fig. 1. The parameters of the proposed method were optimized using grid search as shown in Fig. 2, where we vary p in the range of $\{10, 20, 40, 80, 160, 320\}$ and λ in the range of $\{10^{-4}, 10^{-3}, 10^{-2}, 10^{-1}, 10^{0}, 10^{1}, 10^{2}, 10^{3}, 10^{4}\}$. $\lambda = 10$ and $p = 10$ are selected as the optimal parameters for *Indian Pines*. The results in Table 1 demonstrate that JSSC achieves the best OA and κ with a significant improvement over others. In comparison with SSC and L2-SSC, JSSC gets 21.29% and 18.62% enhancements of OA, respectively.

Experiment 2 was conducted on an urban HSI: *Pavia University*, which was acquired by the Reflective Optics System Imaging Spectrometer (ROSIS) sensor during a flight campaign over Pavia, Northern Italy. An image with size of 200×100 is extracted as the test data that includes 8 classes in total.

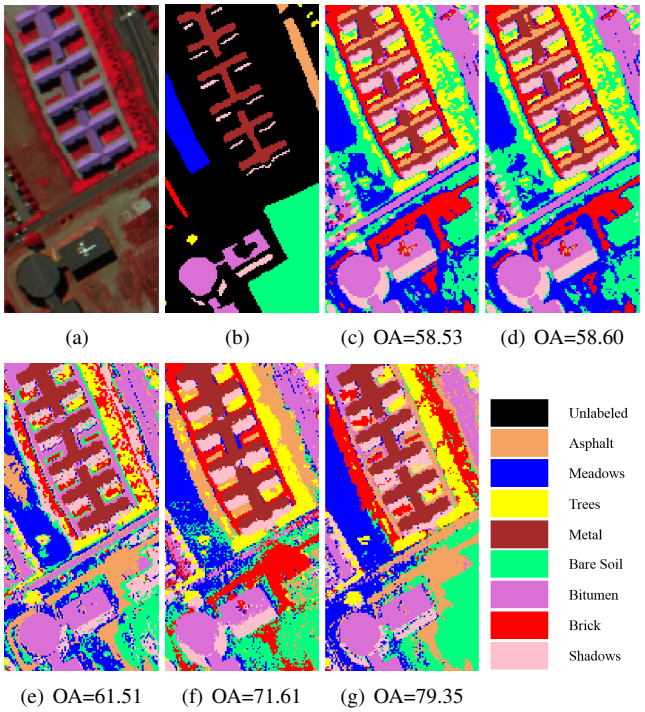

Fig. 3. *Pavia University* image. (a) False color image, (b) Ground truth, and Clustering maps of (c) FCM (d) k-means. (e) SSC. (f) L2-SSC. (g) JSSC.

The false color image and ground truth can be found in Fig. 3 (a) and (b). The OA with respect to λ and p are shown in Fig. 2. We set $\lambda = 10$ and $p = 80$ as the optimal parameters. The results are reported in Table 2 and Fig. 3. JSSC yields again the best performance in terms of OA and κ, with 17.84% and 7.74% improvement of OA over SSC and L2-SSC, respectively. Fig. 3 shows that the clustering results of JSSC are more accurate and smoother than others with joint sparsity constraint in the local regions, which leads to a more precise construction of the similarity matrix. Moreover, results in Fig. 2 indicate a stable and good performance of JSSC with $\lambda = 10$ and $p_n \in [17, 67]$ for both data.

5. CONCLUSION

In this paper, we proposed a joint sparsity based sparse subspace clustering for hyperspectral images. The local information of HSI is first extracted by a super-pixel segmentation technique and further employed in the subspace-sparse representation, which greatly promotes the connectivity of the similarity matrix, leading to a superior clustering performance. An optimization algorithm based on ADMM is also derived for the resulting JSSC model. Experimental results on two real HSIs reveal a significant improvement over the state-of-the-art methods, which confirms the effectiveness of the proposed model.

6. REFERENCES

[1] M. T. Eismann, A. D. Stocker, and N. M. Nasrabadi, "Automated hyperspectral cueing for civilian search and rescue," *Proceedings of the IEEE*, vol. 97, no. 6, pp. 1031–1055, 2009.

[2] B. Datt, T. R. McVicar, T. G. Van Niel, D. L. Jupp, and J. S. Pearlman, "Preprocessing eo-1 hyperion hyperspectral data to support the application of agricultural indexes," *IEEE Trans. Geosci. Remote Sens.*, vol. 41, no. 6, pp. 1246–1259, 2003.

[3] G. Camps-Valls, D. Tuia, L. Bruzzone, and J. A. Benediktsson, "Advances in hyperspectral image classification: Earth monitoring with statistical learning methods," *IEEE Signal Process. Mag.*, vol. 31, no. 1, pp. 45–54, 2014.

[4] H. Zhang, H. Zhai, L. Zhang, and P. Li, "Spectral–spatial sparse subspace clustering for hyperspectral remote sensing images," *IEEE Trans. Geosci. Remote Sens.*, vol. 54, no. 6, pp. 3672–3684, 2016.

[5] S. Lloyd, "Least squares quantization in pcm," *IEEE Trans. Inf. Theory*, vol. 28, no. 2, pp. 129–137, 1982.

[6] J. C. Bezdek, "Pattern recognition with fuzzy objective function algorithms," 1981.

[7] R. Vidal, Y. Ma, and S. Sastry, "Generalized principal component analysis (GPCA)," *IEEE Trans. Pattern Anal. Mach. Intell.*, vol. 27, no. 12, pp. 1945–1959, 2005.

[8] H. Zhang, Q. Wang, W. Shi, and M. Hao, "A novel adaptive fuzzy local information c-means clustering algorithm for remotely sensed imagery classification," *IEEE Trans. Geosci. Remote Sens.*, 2017.

[9] E. Elhamifar and R. Vidal, "Sparse subspace clustering: Algorithm, theory, and applications," *IEEE Trans. Pattern Anal. Mach. Intell.*, vol. 35, no. 11, pp. 2765–2781, 2013.

[10] W. Sun, L. Zhang, B. Du, W. Li, and Y. M. Lai, "Band selection using improved sparse subspace clustering for hyperspectral imagery classification," *IEEE J. Sel. Topics Appl. Earth Observ. in Remote Sens.*, vol. 8, no. 6, pp. 2784–2797, 2015.

[11] H. Zhai, H. Zhang, L. Zhang, P. Li, and A. Plaza, "A new sparse subspace clustering algorithm for hyperspectral remote sensing imagery," *IEEE Geosci. Remote Sens. Lett.*, vol. 14, no. 1, pp. 43–47, 2017.

[12] H. Zhai, H. Zhang, X. Xu, L. Zhang, and P. Li, "Kernel sparse subspace clustering with a spatial max pooling operation for hyperspectral remote sensing data interpretation," *Remote Sensing*, vol. 9, no. 4, pp. 335, 2017.

[13] A. Y. Ng, M. I. Jordan, and Y. Weiss, "On spectral clustering: Analysis and an algorithm," in *Advances in neural information processing systems*, 2002, pp. 849–856.

[14] H. Zhai, H. Zhang, L. Zhang, and P. Li, "Reweighted mass center based object-oriented sparse subspace clustering for hyperspectral images," *Journal of Applied Remote Sensing*, vol. 10, no. 4, pp. 046014, 2016.

[15] E. Elhamifar and R. Vidal, "Sparse subspace clustering," in *Proc. IEEE CVPR*, 2009, pp. 2790–2797.

[16] S. Boyd, N. Parikh, E. Chu, B. Peleato, and J. Eckstein, "Distributed optimization and statistical learning via the alternating direction method of multipliers," *Foundations and Trends® in Machine Learning*, vol. 3, no. 1, pp. 1–122, 2011.

[17] H. Zhang, J. Li, Y. Huang, and L. Zhang, "A nonlocal weighted joint sparse representation classification method for hyperspectral imagery," *IEEE J. Sel. Topics Appl. Earth Observ. in Remote Sens.*, vol. 7, no. 6, pp. 2056–2065, 2014.

[18] L. Fang, S. Li, X. Kang, and J. A. Benediktsson, "Spectral–spatial classification of hyperspectral images with a superpixel-based discriminative sparse model," *IEEE Trans. Geosci. Remote Sens.*, vol. 53, no. 8, pp. 4186–4201, 2015.

[19] W. Fu, S. Li, L. Fang, X. Kang, and J. A. Benediktsson, "Hyperspectral image classification via shape-adaptive joint sparse representation," *IEEE J. Sel. Topics Appl. Earth Observ. in Remote Sens.*, vol. 9, no. 2, pp. 556–567, 2016.

[20] S. Huang, H. Zhang, and A. Pižurica, "A robust sparse representation model for hyperspectral image classification," *Sensors*, vol. 17, no. 9, pp. 2087, 2017.

[21] M. Liu, O. Tuzel, S. Ramalingam, and R. Chellappa, "Entropy rate superpixel segmentation," in *Proc. IEEE CVPR*, 2011, pp. 2097–2104.

[22] E. J. Candès, X. Li, Y. Ma, and J. Wright, "Robust principal component analysis?," *Journal of the ACM (JACM)*, vol. 58, no. 3, pp. 11, 2011.

[23] S. Shekhar, V. M. Patel, N. M. Nasrabadi, and R. Chellappa, "Joint sparse representation for robust multimodal biometrics recognition," *IEEE Trans. Pattern Anal. Mach. Intell.*, vol. 36, no. 1, pp. 113–126, 2014.